ADVANCES IN ATMOSPHERIC SCIENCES, VOL. 28, NO. 1, 2011, 118–128

Numerical Study of the Mesoscale Systems in the Spiral Rainband of 0509 Typhoon Matsa

ZHOU Lingli*[1,2] (周玲丽), ZHAI Guoqing[1] (翟国庆), and HE Bin[3] (何 斌)

[1] *Department of Earth Sciences, Zhejiang University, Hangzhou* 310027

[2] *Zhejiang Province Meteorological Observatory, Hangzhou* 310017

[3] *Jiaxing Meteorological Observatory, Jiaxing* 314001

(Received 3 Feburary 2010; revised 13 April 2010)

ABSTRACT

The Advanced Weather Research and Forecasting Model (ARW) is used to simulate the local heavy rainstorm process caused by Typhoon Matsa over the northeastern coast of Zhejiang Province in 2005. The results show that the rainstorm was caused mainly by the secondary spiral rainband of the Stationary Band Complex (SBC) structure. Within the secondary spiral rainband there was a strong meso-β-scale convergence line generated in the boundary layer, corresponding very well to the Doppler radar echo band. The convergence line comprised several smaller convergence centers, and all of these convergence columns inclined outward. Along the convergence line there was precipitation greater than 20 mm occurring during the following one hour. During the heavy rainstorm process, the Doppler radar echo band, convergence line, and the precipitation amount during the following one hour, moved and evolved synchronously. Further study reveals that the vertical shear of radial wind and the low-level jet of tangential wind contributed to the genesis and development of the convergence columns. The combined effect of the ascending leg of the clockwise secondary circulation of radial wind and the favorable environment of the entrance region of the low-level jet of tangential wind further strengthened the convergence. The warm, moist inflow in the lower levels was brought in by the inflows of the clockwise secondary circulation and uplifted intensely at the effect of convergence. In the convectively instable environment, strong convection was triggered to produce the heavy rainstorm.

Key words: typhoon rainstorm, convergence line, spiral rainband, radial wind, tangential wind

Citation: Zhou, L. L., G. Q. Zhai, and B. He, 2011: Numerical study of the mesoscale systems in the spiral rainband of 0509 Typhoon Matsa. *Adv. Atmos. Sci.*, **28**(1), 118–128, doi: 10.1007/s00376-010-0023-2.

1. Introduction

China is one of the most seriously affected countries in the world by typhoons, with an average of seven to eight landfalling typhoons per year (Chen and Ding, 1979). Typhoon disasters top all other natural disasters in terms of their frequency and degree of influence in coastal areas. This is mainly brought about by their associated rainstorms, and one of the most important weather systems leading to a typhoon rainstorm is the spiral rainband. These rainbands are typically 5–50-km wide and 100–300-km long, are ubiquitous in tropical cyclones, and have a complex 3D structure with extensive stratiform rain areas embedded with deep convective cores (e.g. Atlas et al., 1963; Barnes et al., 1983; Barnes et al., 1991). Many studies have demonstrated the significant role of these deep, small-scale convective systems in severe heavy rain associated with typhoons (Chen, 1995; Chen and Luo, 1995; Meng et al., 1996). The precipitation generated by small convective systems is often heavier than that produced by the typhoon circulation itself, and directly affects the intensity and distribution of the rain (Cheng et al., 2005). Past research has also found a close connection between mesoscale heavy rainfall and strong radar echo in typhoons, both of which correspond to significant convergence in the boundary layer (Zhou, 2008; Zhou et al., 2009).

*Corresponding author: ZHOU Lingli, zhoulingli_1231@sohu.com

In recent years, Zhejiang Province, one of the most economically-advanced and populous areas on China's southeast coast, has been affected seriously by heavy rainstorms brought about by landfalling typhoons. On average, there are 5.3 tropical cyclones affecting Zhejiang Province per year, 0.66 of which land in the province itself (Yang et al., 2007). The total rainfall recorded at an individual station in Zhejiang Province during a typhoon event is generally larger than 100 mm, and to date there have been 31 typhoons which have produced a maximum total rainfall of greater than 500 mm (Lü and Yao, 2006). For example, 0509 Typhoon Matsa, which landed in Yuhuan on the southeast coast of Zhejiang Province at 1940 UTC 05 August 2005, led to an extraordinary rainstorm over the north coast of the province. The maximum total rainfall of an individual station during this typhoon was in excess of 511.5 mm, which impacted heavily in terms of economic loss, as well as the number of injuries and fatalities caused. The infrared satellite cloud pictures of Typhoon Matsa as it landed show there were two other strong cloud bands located cyclonically outside the eyewall (Fig. 1). According to Willoughby et al. (1984), this is the typical structure of a Stationary Band Complex (SBC), which includes a principal band, a connecting band linking the inner eyewall and the outer rainband, and occasionally a secondary rainband between the eyewall and the outer principal rainband. For Typhoon Matsa, the secondary rainband was the main system contributing to the heavy rainstorm over the northeastern coast of Zhejiang Province.

Although the importance of convective-scale systems in tropical cyclones has been argued convincingly (Riehl and Malkus, 1958), few studies have focused on this area. The reason for this is mainly because of the short life cycle and rapid development of small-scale convective systems. It is difficult to study directly and deeply the internal structure of these systems using existing observational methods. However, Doppler radar observation and numerical simulation have become very helpful and advantageous tools to study the interior structure of typhoon mesoscale rainstorms, particularly given recent improvements in the coastal layout of Doppler radar and developments in numerical weather forecasting. In order to further understand the genesis and developmental mechanisms of typhoon heavy rainstorms, as well as the structural features of mesoscale convective systems in the spiral rainband, the mesoscale numerical model, WRF (Weather Research and Forecasting Model), is used in this paper to reproduce and study the rainstorm processes caused by Typhoon Matsa.

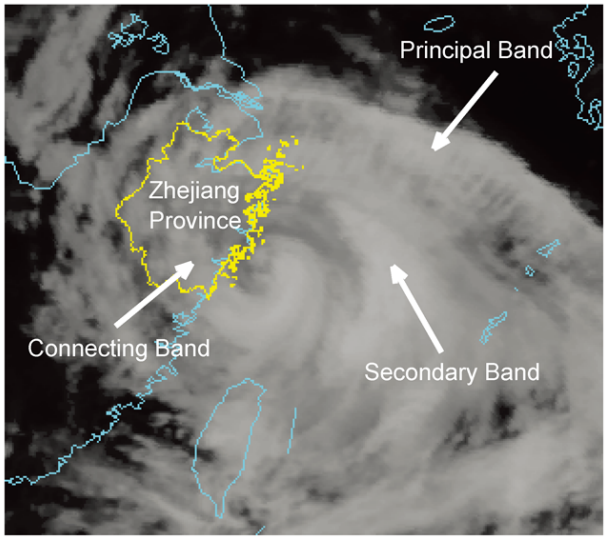

Fig. 1. FY2C infrared satellite picture at 1600 UTC 5 August 2005.

2. Case and experiment design

The numerical simulation was conducted using the Advanced Research WRF (ARW) mesoscale model. The ARW, with two nested domains (Fig. 2), was used to perform a 48-h simulation, starting from 0000 UTC 05 August 2005, 24 hours before the rainstorm. The model was run with 31 vertical levels in the terrain-following σ coordination. The horizontal grid spacing of the first mesh was 30 km, with 121×110 grid points. The horizontal grid spacing of the second mesh was 10 km, with 91×88 grid points. The initial and lateral boundary conditions were based on the six-hourly (0000, 0600, 1200, 1800 UTC) NCEP Final Analysis data with a resolution of 1°. The microphysics scheme

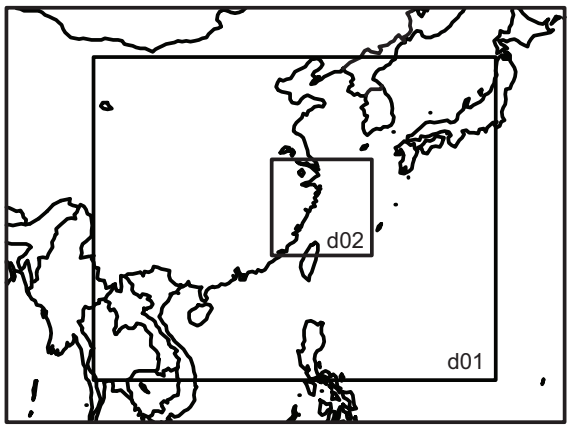

Fig. 2. The two nested domains of the numerical experiments.

used in the model was the Lin et al. scheme (Lin et al., 1983; Rutledge and Hobbs, 1984; Tao, 1989). The cumulus option was parameterized with the Betts-Miller-Janjic scheme (Betts, 1986; Betts and Miller, 1986; Janjic, 1994), and the Yonsei University boundary layer scheme (Hong and Dudhia, 2003) is adopted.

In the designed experiment, a cycling assimilation model, WRF-Var, was used to assimilate observation data every six hours. In this approach, the first guess for WRF-Var was the six-hour short-range WRF forecast initialized from the previous WRF-Var analysis. The covariance matrix for WRF-Var was obtained from the statistics of previous WRF forecasts for a month by the NMC (National Meteorological Center) method (Barker et al., 2001; Parrish and Derber, 1992). The observations used for the assimilation included conventional surface observations and upper air observations, as well as radar reflectivity and radial velocity data.

3. Results and verification

3.1 *Typhoon track*

The observed track (solid line in Fig. 3) shows that Typhoon Matsa moved northwestward and hit the southeastern coast of Zhejiang Province (28°N, 121.2°E) at 1940 UTC 5 August 2005, then kept travelling northwestward across the province, before finally leaving at 1400 UTC 6 August 2005. Comparing the simulated track (dotted line in Fig. 3), the result shows

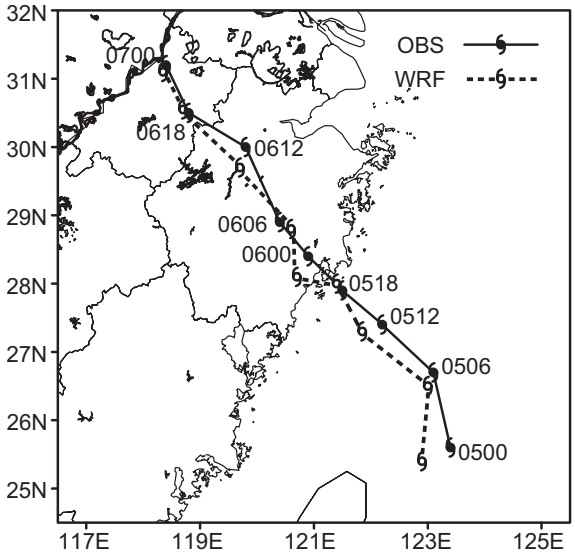

Fig. 3. Observed and simulated tracks of Typhoon Matsa. The solid line represents the observed track from the best track of CWB, and the dotted line represents the simulated track from WRF.

that, except for some slight northward and southward deflection, the simulated track is in general agreement with the best-track analysis from CWB (Central Weather Bureau of Taiwan). The position of the simulated typhoon center deflects about 10–15 km southward from the observation before landing, and debarks one hour earlier at about 10 km south from the observed landing spot. However, the simulated typhoon then also moves northwestward, leaving Zhejiang Province at the same time and same place as the observation.

3.2 *Precipitation*

Before describing the observed precipitation pattern, it is important to note that the data were obtained from automatic surface weather stations, meaning there were no data for sea areas. It can be seen in Fig. 4a that there was heavy rainfall distributed from southeast to northwest over the northeastern coast of Zhejiang Province, which amounted to 350 mm of rainfall in 24 hours. The rain was highly centralized, with rainfall of greater than 300 mm limited to within 150 km in every direction. The simulation result is generally consistent with the observation (Fig. 4). As observed, there is also a strong centralized rain belt extending from southeast to northwest over the northeastern coast of Zhejiang Province, although its position is about 10 km south and the maxima are a bit weaker than the observation (Fig. 4b).

The above results indicate that the simulation was basically consistent with observation, meaning the model can generally reflect the rainstorm processes of this typhoon. Therefore, simulated results can be used for further analysis.

4. The spiral rainband and mesoscale convergence line in the boundary layer

Some studies have found that heavy rainstorms caused by certain typhoons are related closely to the mesoscale convergence line in the boundary layer. The convergence line plays an important role in the forming, triggering and maintaining of heavy rainstorms (Zhou, 2008; Zhou et al., 2009). To check this assertion for the case of Typhoon Matsa, observed Doppler radar echo data, as well as AWS (Automatic Weather Station) precipitation data, were compared with the simulated convergence field to investigate the connection between these three elements.

At 0600 UTC (Fig. 5a), there was a strong radar echo band larger than 35 dBZ appearing to the northeast of the typhoon center over the northeastern coast of Zhejiang Province. The echo band was about 250-km long and 25-km wide, running from southeast to

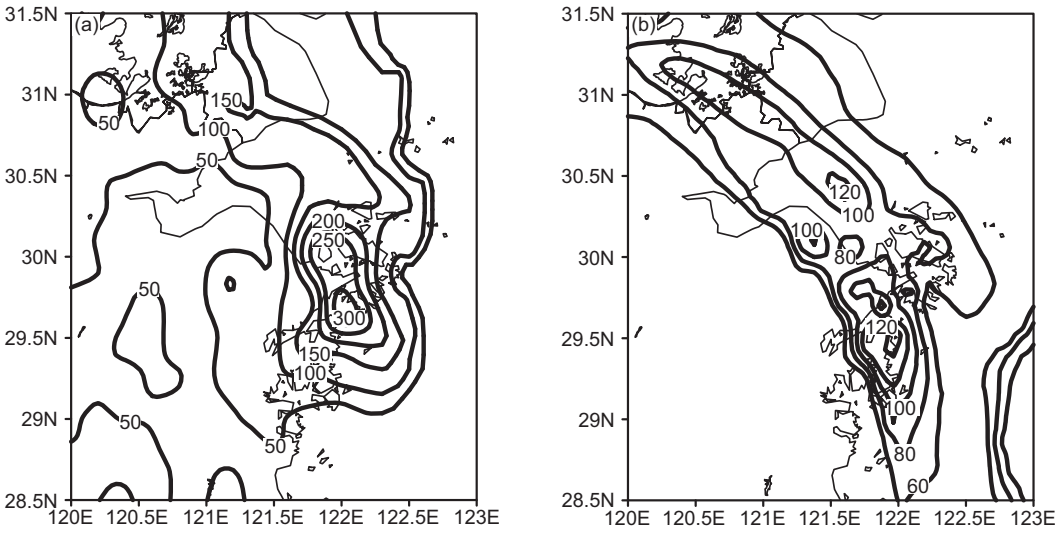

Fig. 4. Accumulated 24 h precipitation of Typhoon Matsa (mm): (a) accumulated precipitation from AWS from 0000 UTC 6 to 0000 UTC 7 August 2005; (b) simulated precipitation from 24 h to 48 h.

northwest. Along the band, there were several echo centers of 45–55 dBZ embedded in line, which corresponded to the secondary spiral rainband of Typhoon Matsa. Outside the strong echo band, there was another radar echo band occurring over the sea. Although the outer echo band was also composed of a few echo centers, its intensity was much weaker and the structure was relatively looser. It was the principal rainband that the outer echo band corresponded to. Inside the two radar echo bands, there were a few echo blocks extending to the eyewall along the radial, which corresponded to the connecting spiral rainband. During the next hour, AWS precipitation mainly occurred within the secondary rainband, amounting to more than 20 mm. The course and position of the rain maxima both corresponded very well to the secondary rainband. Many studies have found rainbands to the east of a typhoon center move slowly outward along the radial (Senn and Hiser, 1959; Willoughby, 1978; May, 1996), and may remain stationary with new cells forming on the upwind edge (Atlas et al., 1963). In the process of propagating outward, the principal rainband sometimes decays and dies out, being replaced by the secondary rainband which develops and then becomes the new principal rainband (May, 1996). This very thing happened to the spiral ranbands of Typhoon Matsa during the next couples of hours (Figs. 5c, 5e, 5g, and 5i). The position of the spiral rainbands basically remained still over the northeastern coast of Zhejiang Province while Typhoon Matsa was moving northwestward, demonstrating that both the rainbands were propagating outward radially. However, the evolution tendency of these two rainbands was totally opposite. The secondary rainband intensified significantly while moving outward, with new small echo bulks constantly born in the upper end (upwind edge) of the echo band. On the contrary, the principal rainband outside gradually weakened, and finally died out to be replaced by the secondary rainband. During this process, not only did the next occurrence of AWS precipitation still correspond very well to the secondary rainband, but it also gained significant amplification with the development of secondary rainband. The one-hour rain maxima rapidly increased to over 100 mm from 20 mm in only three to four hours.

The simulated convergence field at 925 hPa reveals strong convergence lines near the area of observed radar echo bands. The convergence lines belong to the meso-β-scale and have a similar course and structure to the echo bands. Although there is some deflection between the position of the convergence lines and echo bands because of inevitable errors in the numerical model, the evolution and structural characteristics demonstrate that the simulated convergence lines and observed radar echo bands all represent the spiral rainbands. Figure 5b shows that the simulated convergence line corresponding to the secondary spiral rainband is relatively strong at 0600 UTC, composed of three or four meso-γ-scale strong convergence centers over -35×10^{-5} s^{-1}. However, the convergence line outside corresponding to the principal spiral rainband is much weaker, -12×10^{-5} s^{-1} at most, and has a loose structure. In the area between the convergence lines and the typhoon center, there are also several small convergence centers along the radial, corresponding to the connecting spiral rainband. Then,

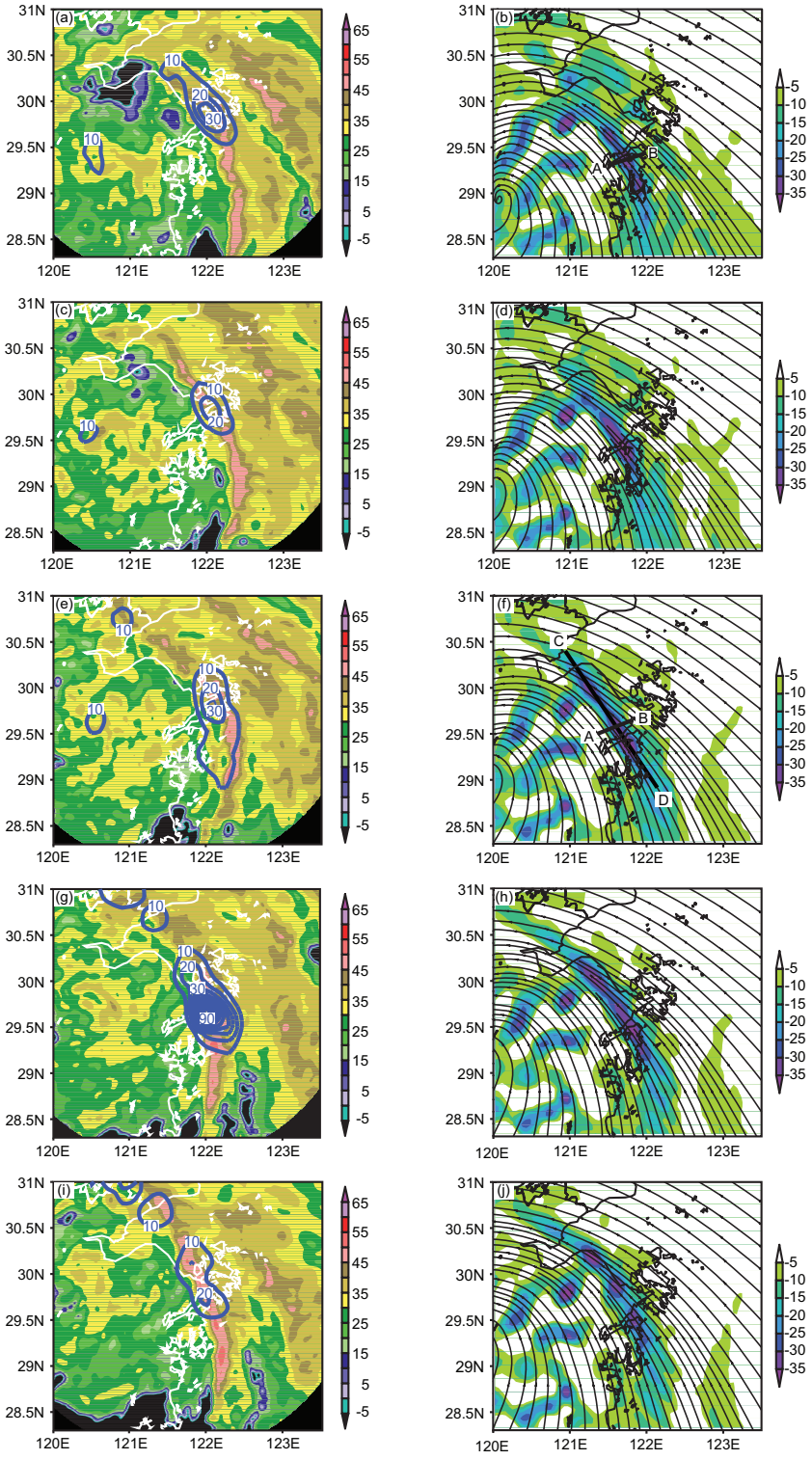

Fig. 5. Observed CAPPI echo of Ningbo Doppler Radar at a height of 0.5 km (dBZ) and simulated convergence field ($\times 10^{-5}$ s^{-1}) with stream line at 925 hPa: (a) and (b) 0600 UTC 6 August 2005; (c) and (d) 0700 UTC 6 August 2005; (e) and (f) 0800 UTC 6 August 2005; (g) and (h) 0900 UTC 6 August 2005; (i) and (j) 1000 UTC 6 August 2005. The blue contour represents precipitation during the next one hour, colored shading in the left column indicates Doppler radar echo over 35 dBZ, and colored shading in the stream field represents convergence stronger than -10×10^{-5} s^{-1}.

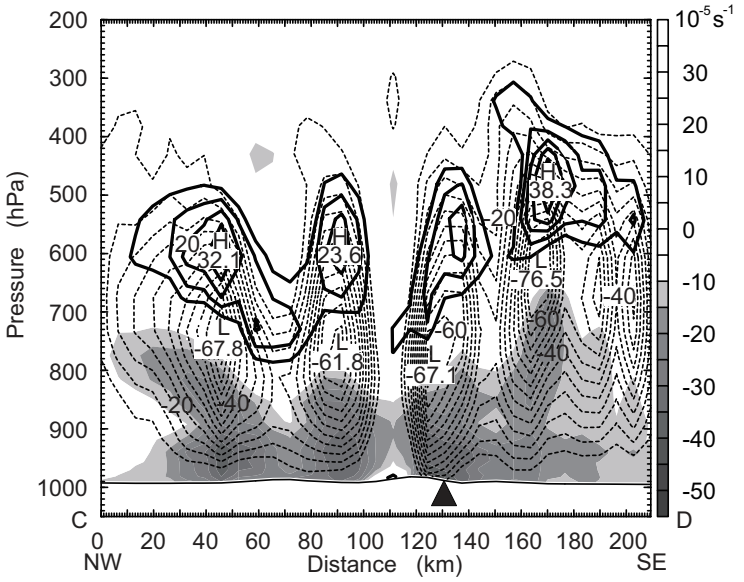

Fig. 6. Vertical cross section along the convergence line at 0800 UTC 6 August 2005. Shading represents convergence over -10×10^{-5} s^{-1}; the solid contour represents divergence greater than 10×10^{-5} s^{-1}; dotted lines represent ascending velocity ($\times10^{-3}$ hPa s^{-1}), and the black triangle marks the position of the convergence center leading to the local heavy rainstorm over the northeastern coast of Zhejiang Province. The line C–D can be seen in Fig. 5j.

both of the convergence lines move gradually outward in a radial fashion, with the convergence line inside intensifying and the convergence line outside decaying and dying out in two hours (Figs. 5d and 5f). Finally, the inner convergence line takes the place of the convergence line outside (Figs. 5h and 5j).

The above analysis reveals that the SBC to the east of the center of Typhoon Matsa was the main effect system of the rainstorm process, which consisted of several rain cells with a much smaller scale. The secondary spiral rainband of the SBC in particular was the direct effect system contributing to the heavy rainstorm over the northeastern coast of Zhejiang Province. The secondary spiral rainband moved gradually outward and intensified, then became the new principal spiral rainband after the old one died out. There were stable strong meso-β-scale convergence lines corresponding to the spiral rainbands in the boundary layer, which had a similar scale, course, distribution and development tendency to the spiral rainbands. Along the secondary spiral rainband, there was heavy rainfall of over 20 mm produced during the next hour. The rainfall distributed and evolved synchronically with the convergence line. The above results prove further the credibility of the simulated convergence field.

5. Vertical structure of the mesoscale convergence line in the spiral rainband

In section 4, the low-level convergence field was shown to have a strong mesoscale convergence line closely related to the secondary spiral rainband. In this section, the vertical structure is investigated in order to discover the development mechanism of the convergence line.

Figure 6 presents a vertical cross section along the convergence line at 0800 UTC 6 August 2005. As can be seen, there are four convergence cells lining from southeast to northwest along the convergence line. The convergence maxima appear below 900 hPa and the top of the convergence cells reach up to 650–750 hPa. At 400–700 hPa there are four divergence cells, forming four one-to-one structures together with the convergence cells, respectively. This suggests that strong ascending flows occurred between the div-convergence cells at the effect of pumping and lift-up, with the largest ascending velocity exceeding -60×10^{-3} hPa s^{-1}.

Figure 7 shows the development process of the vertical cross section transecting the convergence line and passing through one convergence center, which led to the local heavy rainstorm over the northeastern coast

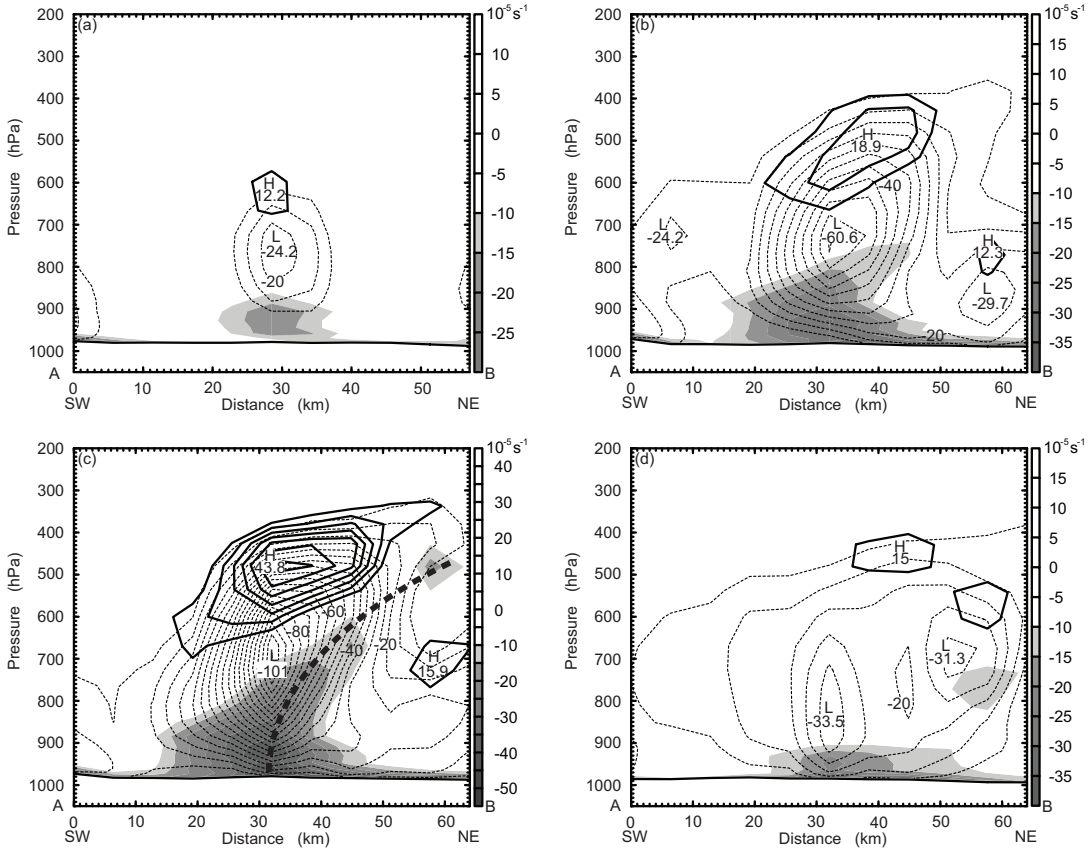

Fig. 7. Vertical cross section transecting the convergence line and passing through the convergence center that led to the local heavy rainstorm over the northeastern coast of Zhejiang Province at (a) 0400 UTC; (b) 0600 UTC; (c) 0800 UTC; and (d) 1400 UTC 6 August 2005. The shading represents convergence over -10×10^{-5} s^{-1}; the solid line represents divergence greater than 10×10^{-5} s^{-1}; the dotted lines show ascending velocity ($\times10^{-3}$ hPa s^{-1}); and the black bold dashes in (c) marks the axis line of one convergence cell. The line A–B can be seen in Fig. 5f, and moved with the convergence line over time.

of Zhejiang Province (indicated by the black triangle in Fig. 6). The cross line is positioned toward the typhoon's center and moves with the convergence line over time. The convergence is weak in the initial phase. There is only a weak convergence center below -20×10^{-5} s^{-1} near the surface, and some weak divergence drafts at 600 hPa. The ascending flow between the convergence and divergence centers are also so weak that there only a small amount of scattered rainfall appears in this area (Fig. 7a). After two hours (Fig. 7b), the convergence strengthens rapidly and gradually develops on an upward incline to the outside of the typhoon. The divergence zone over the convergence center also lifts significantly, and intensifies. As a result, the ascending movement gains further force to produce heavier rain. At 0800 UTC (Fig. 7c), the convergence reaches its peak, forming a strong inclining convergence column from the surface to 450 hPa, with a maximum over -50×10^{-5} s^{-1}. The divergence above develops significantly and, in addition, the ascending velocity reaches its largest intensity of -100×10^{-3} hPa s^{-1}. Such a mature stage is maintained for around three to four hours, during the stage when the rainfall increases greatly. After that, the convergence starts to decay, as do the divergence and ascending drafts. Rainfall then decreases to the end of the event (Fig. 7d).

6. The cause of the convergence line and heavy rainstorm in the secondary spiral rainband

The distribution and evolution of the wind field have an important influence on the genesis and development of convergence, since the genesis of convergence is mainly the result of the accumulation of air particles, which itself results from the non-uniform distribution of airflow.

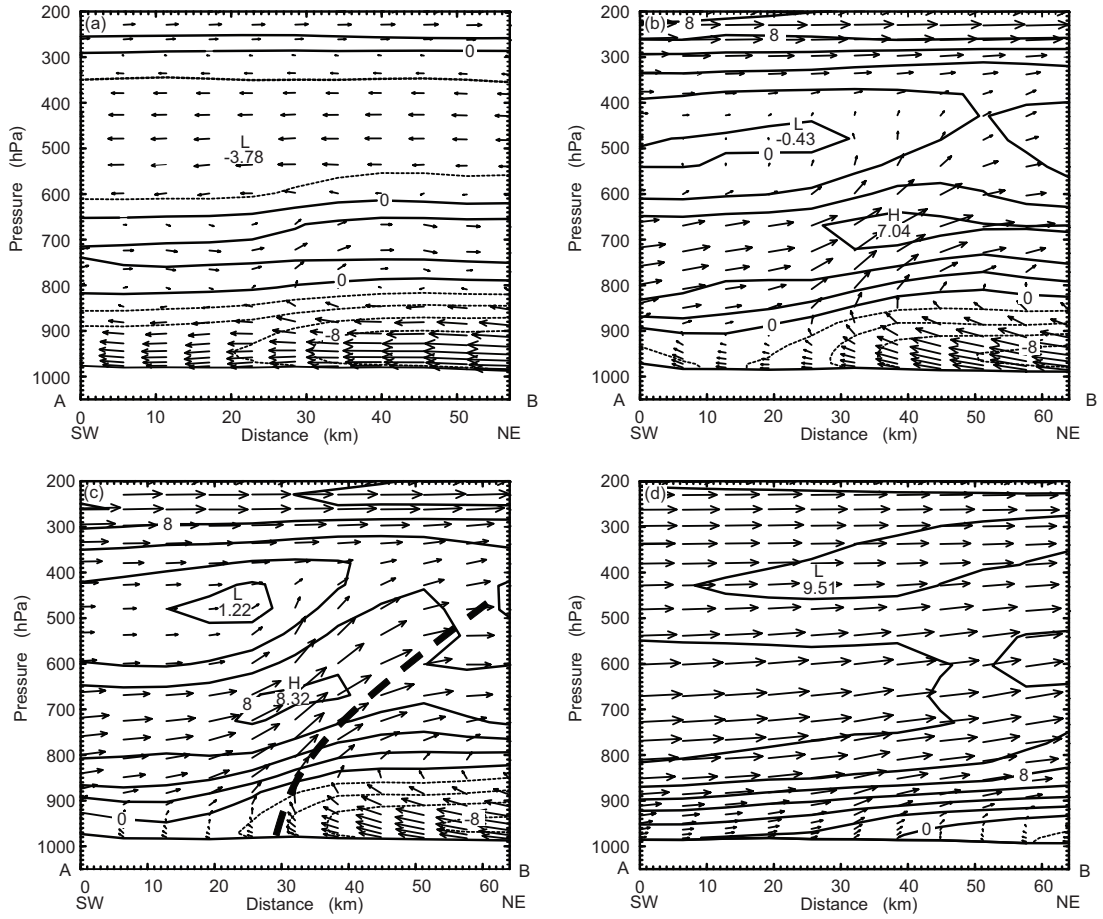

Fig. 8. Vertical structure of radial wind (m s^{-1}) at different development stages of the convergence: (a) 0400 UTC; (b) 0600 UTC; (c) 0800 UTC; (d) 1400 UTC 6 August 2005. The contour represents radial wind velocity, and the black bold dashes in (c) mark the axis line of one convergence cell. The line A–B is the same as in Fig. 7.

The distribution and evolution of the radial wind field at different convergence development stages were investigated in order to understand the specific reason for the formation of convergence. During the initial stage of the rainstorm (Fig. 8a), almost all air in the entire troposphere is inflowing; only one air current can be see flowing outward, at 700–800 hPa. The maximum velocity of the inflow is about -8 m s^{-1}, appearing in the area approximately 40–50 km outside the rainband at 950 hPa, and decreasing slowly along the radial toward the typhoon center in the boundary layer. Consequently, there weak convergence occurs on the inner side of the velocity maxima of the inflows. In addition, a small weak disturbance starts to occur at the border of the inflow in the boundary layer and the outflow in the middle and low levels around 800 hPa, forming a clockwise secondary circulation between them.

At 0600 UTC (Fig. 8b), the inflow at the outer side of the rainband in the boundary layer weakens slightly, while the outflow in the mid troposphere strengthens significantly, with its maximum velocity reaching 7 m s^{-1}. This is due to the typhoon being dissipated by the land surface as it moves inland. The structure of the typhoon becomes looser and weaker, leading to more and more outflows in the middle and upper troposphere. The radial wind velocity changes from -8 m s^{-1} to 7 m s^{-1} within an altitude of only 3 km, which offers a strong sheared environment advantageous to the formation and maintaining of a spiral rainband (Barnes et al., 1983). The convergence line corresponding to the rainband develops rapidly during this period. With the common action of convergence uplift and divergence pumping, the clockwise secondary circulation in the lower troposphere intensifies further, making the ascending movement within the rainband more intense. Meanwhile, the maximum outflow velocity in the mid troposphere also increases, to over 8 m s^{-1} (Fig. 8c). All of these factors strengthen the vertical wind shear, causing the spiral rainband and

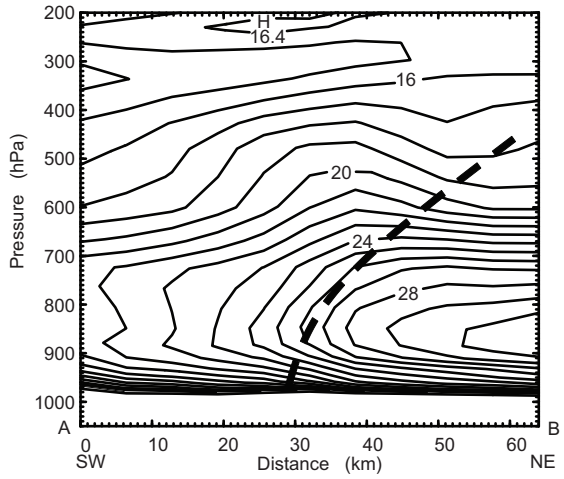

Fig. 9. Vertical structure of tangential wind (m s^{-1}) at 0800 UTC 6 August 2005. The contour represents tangential wind velocity, and the black bold dashes mark the axis line of one convergence cell. The line A–B is the same as in Fig. 7c.

convergence line to keep developing upwards.

At 1400 UTC (Fig. 8d), lower level inflow decreases quickly as the typhoon moves further inland, while the outflow in middle levels increases to 12 m s^{-1} and the clockwise secondary circulation on the outer side of the rainband disappears. As a result, the ascending movement is suppressed, subsequently subduing the spiral rainband and convergence line, before finally dying out. According to the wind field at 700 hPa (figure not shown), the east wind jet in the outer typhoon pierces through the vertical cross section when rotating cyclonically with the typhoon circulation. Therefore, the maximum wind outflow appearing in the middle levels probably forms from the east wind jet, which is ubiquitous in the spiral rainband (Samsury and Zipser, 1995; May, 1996).

Since the tangential wind is much stronger, its contribution to the development of the convergence cannot not be ruled out. Figure 9 shows a strong low-level jet between 950 hPa and 850 hPa in the area 40 km outside the rainband at 0800 UTC, with the maximum velocity of the jet being greater than 30 m s^{-1}. In fact, the low-level jet remains consistent throughout the rainstorm process (figure not shown). The convergence center is located just in the left side of the entrance region, creating an advantageous environment for the genesis and development of convergence. Besides, the ascending leg of the clockwise secondary circulation in Fig. 8 happens to be in the entrance region of the low-level jet, and this ascending movement could further promote low-level convergence.

The equivalent potential temperature field (Fig. 10a) shows a high value area within the convergence zone in the rainband. Flows below 850 hPa are all warm and moist, with equivalent potential temperature greater than 358 K. Furthermore, there is a warm tongue bumping upward corresponding to the convergence column. In the areas of radial inflow and strongest updraft, there is negative equivalent potential temperature advection, and the strongest negative advection occurs in the latter, reaching -14.3×10^{-4} K s^{-1}. When the updrafts ascend to 700 hPa and flow outward, the equivalent potential temperature advection then converts to positive and generates a maximum of 15.2×10^{-4} K s^{-1}. From this it can be judged that, when the state of the middle and lower levels of the troposphere are convectively instable (Fig. 10b),

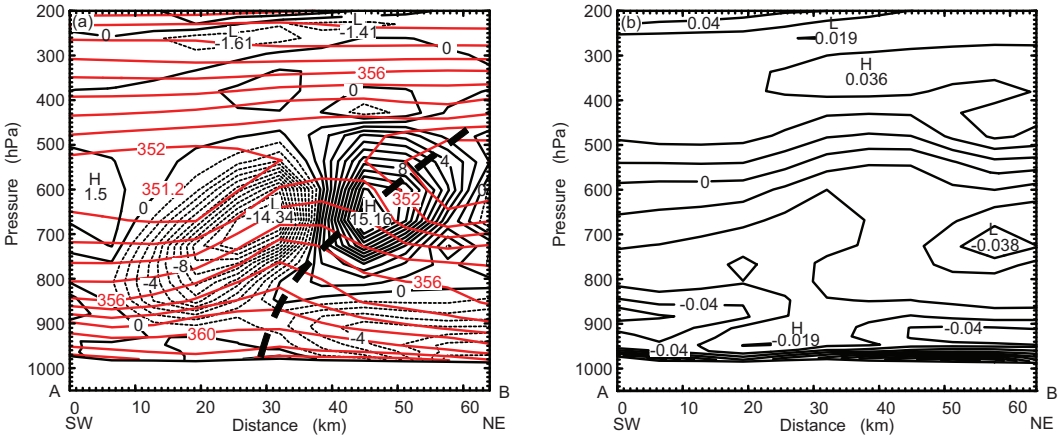

Fig. 10. Vertical structure of (a) equivalent potential temperature field (red contour, K) and advection (black contour, $\times10^{-4}$ K s^{-1}), and (b) convective stability index ($-\partial\theta/\partial p$, K hPa^{-1}) at 0800 UTC 6 August 2005. The black bold dashes mark the axis line of one convergence cell. The line A–B is the same as in Fig. 7. When $-\partial\theta/\partial p$ <0, it is convectively instable.

the inflow toward the convergence line with plenty of moisture and energy uplifts by convergence and triggers strong convection to produce heavy rainfall. During this process, moisture and energy are released. The latent heat of condensation is taken to the middle level by the updraft and then transported outward along the radial by the outflow, making the area outside the rainband warmer than the inside. This is why the warm tongue is inclined outward.

7. Conclusion

The ARW model was used to simulate the local heavy rainstorm process caused by Typhoon Matsa over the northeastern coast of Zhejiang Province in 2005. The results show that:

(1) The rainstorm was mainly caused by the secondary spiral rainband of the SBC structure. Within the secondary spiral rainband, there was a strong meso-β-scale convergence line generated in the boundary layer, corresponding very well to the Doppler radar echo band. The convergence line consisted of several smaller convergence centers which developed upward forming convergence columns, and all of these convergence columns inclined outward. Along the convergence line there was precipitation greater than 20 mm occurring during the following hour. During the heavy rainstorm process, the Doppler radar echo band, convergence line, and the one-hour precipitation amount moved and evolved synchronously.

(2) The vertical shear of radial wind and the low-level jet of tangential wind were the reasons contributing to the genesis and development of the convergence columns. The combined effect of the ascending leg of the clockwise secondary circulation of radial wind and the favorable environment of the entrance region of the low-level jet of tangential wind further strengthened the convergence.

(3) The warm, moist inflow in the lower levels was brought in by the inflows of the clockwise secondary circulation and uplifted intensely at the effect of convergence. In the convectively instable environment, strong convection was triggered to produce the heavy rainstorm.

Acknowledgements. The authors would like to thank ZHA Ben for the conventional observing data, and ZHONG Jianfeng for the Doppler radar data. This work was supported by the State Key Program of the National Natural Science Foundation of China (Grant No. 40830958), the Research Project of Serious Oceanic Disasters Alerting and Application Technology (Grant No. 2006BAC03B00), the Key Program of the State Key Laboratory of Disaster Weather (Grant No. 2008LASW–A03), and the National Natural Science Foundation of China (Grant No. 40975021).

REFERENCES

Atlas, D., K. Hardy, R. Wexler, and R. Boucher, 1963: The origin of hurricane spiral bands. *Geofisica Internationale*, **3**, 123–132.

Barker, D., W. Huang, Y. R. Guo, and A. Bourgeois, 2001: A three-dimensional variational (3DVAR) data assimilation system for use with MM5. MMM Division, NCAR, P. O. Box 3000, Boulder, CO, 80307–3000, USA. [Available online from http://www.mmm.ucar.edu/mm53dvar/docs/3DVARTechDoc.pdf.]

Barnes, G. M., E. J. Zipser, D. P. Jorgensen, and F. D. Marks Jr., 1983: Mesoscale and convective structure of a hurricane rainband. *J. Atmos. Sci.*, **40**, 2125–2137.

Barnes, G. M., J. F. Gamache, M. A. LeMone, and G. J. Stossmeister, 1991: A convective cell in a hurricane rainband. *Mon. Wea. Rev.*, **119**, 776–794.

Betts, A. K., 1986: A new convective adjustment scheme. Part I: Observational and theoretical basis. *Quart. J. Roy. Meteor. Soc.*, **112**, 677–691.

Betts, A. K., and M. J. Miller, 1986: A new convective adjustment scheme. Part II: Single column tests using GATE wave, BOMEX, ATEX and arctic air-mass data Sets. *Quart. J. Roy. Meteor. Soc.*, **112**, 693–709.

Chen, L. S., 1995: An overview on tropical cyclones structure and structure change. *Proc. WMO Second International Workshop on Tropical Cyclones, Geneva, Switzerland, WMO,* No. 361, 52–62.

Chen, L. S., and Y. H. Ding, 1979: *An Introduction to Western Pacific Typhoons.* Science Press, Beijing, 491pp. (in Chinese)

Chen, L. S., and Z. X. Luo, 1995: Effect of the interaction of different-scale vortices on the structure and motion of typhoons. *Adv. Atmos. Sci.*, **12**, 207–214.

Cheng, Z. Q., L. S. Chen, X. D. Xu, and T. Y. Peng, 2005: Research progress on typhoon heavy rainfall in China for last ten years. *Meteorological Monthly*, **31**, 3–9. (in Chinese)

Hong, S. Y., and J. Dudhia, 2003: Testing of a new nonlocal boundary layer vertical diffusion scheme in numerical weather prediction applications. *20th Conf. On Weather Analysis and Forecasting/16th Conf. On Numerical Weather Prediction,* Seattle, WA, Amer., Amer. Meteor. Soc., Session 17, WRF Model Development & Applications: Part III.

Janjic, Z. I., 1994: The step-mountain eta coordinate model: Further developments of the convection, viscous sublayer, and turbulence closure schemes. *Mon. Wea. Rev.*, **122**, 927–945.

Lin, Y. L., R. D. Farley, and H. D. Orville, 1983: Bulk parameterization of the snow field in a cloud model. *Journal of Climate and Applied Meteorology*, **22**, 1065–1092.

Lü, Z. P., and Y. W. Yao, 2006: Typhoon disasters in Zhe-

jiang province and the establishment of emergency response mechanism. *Journal of Catastrophology*, **21**, 69–71. (in Chinese)

May, P. T., 1996: The organization of convection in the rainbands of tropical cyclone Laurence. *Mon. Wea. Rev.*, **124**, 807–815.

Meng, Z. Y., M. Nagata, and L. S. Chen, 1996: A numerical study on the formation and development of island-induced cyclone and its impact on typhoon structure change and motion. *Acta Meteorologica Sinica*, **10**, 430–443. (in Chinese)

Parrish, D. F., and J. C. Derber, 1992: The national meteorology center's spectral statistical interpolation analysis system. *Mon. Wea. Rev.*, **120**, 1747–1763.

Riehl, H., and J. S. Malkus, 1958: On the heat balance of the equatorial trough zone. *Geophysica*, **6**, 503–537.

Rutledge, S. A., and P. V. Hobbs, 1984: The mesoscale and microscale structure and organization of clouds and precipitation in midlatitude cyclones. XII: A diagnostic modeling study of precipitation development in narrow cold-frontal rainbands. *J. Atmos. Sci.*, **41**, 2949–2972.

Samsury, C. E., and E. J. Zipser, 1995: Secondary wind maxima in hurricanes: Airflow and relationship to rainbands. *Mon. Wea. Rev.*, **123**, 3502–3517.

Senn, H. V., and H. W. Hiser, 1959: On the origin of hurricane spiral rain bands. *J. Atmos. Sci.*, **16**, 419–426.

Tao, W. K., 1989: An ice-water saturation adjustment. *Mon. Wea. Rev.*, **117**, 231–235.

Willoughby, H. E., 1978: A possible mechanism for the formation of hurricane rainbands. *J. Atmos. Sci.*, **35**, 838–848.

Willoughby, H. E., F. D. Marks, and R. J. Feinberg, 1984: Stationary and moving convective bands in hurricanes. *J. Atmos. Sci.*, **41**, 3189–3211.

Yang, H. J., N. Li, and Y. Lei, 2007: Features of typhoon in southeast coastal regions of China in the recent 54 years. *Scientia Meteorologica Sinica,* **27**, 413–418. (in Chinese)

Zhou, H. G., 2008: 3D structure of the heavy rainfall caused by BILIS (0604) with Doppler radar data. *Chinese J. Atmos. Sci.*, **32**, 1289–1308. (in Chinese)

Zhou, L. L., G. Q. Zhai, D. F. Wang, F. M. Gu, and B. He, 2009: Numerical simulation and analysis of Typhoon Haitang (0505) heavy rainfall. *Chinese J. Atmos. Sci.*, **33**, 489–500. (in Chinese)